JOURNAL OF GEOPHYSICAL RESEARCH, VOL. 96, NO. B7, PAGES 12,245–12,255, JULY 10, 1991

Deformation of the Central Andes (15°–27°S) Derived From a Flow Model of Subduction Zones

SHIMON WDOWINSKI[1] AND RICHARD J. O'CONNELL

Department of Earth and Planetary Sciences, Harvard University, Cambridge, Massachusetts

A simple viscous flow model of a subduction zone is used to calculate the deformation within continental lithosphere above a subducting slab. Our formulation accounts for two forces that dominate the deformation in the overriding lithosphere: tectonic forces and buoyancy forces. The tectonic forces arise from the subduction of oceanic lithosphere and produce minor extension in the lithosphere near the trench and compression farther inland. Buoyancy forces can induce horizontal pressure gradients due to variations in crustal thickness, which cause lithospheric extension where the crust is thick. Numerical solutions, obtained by using a finite element technique, are compared with observations from the central Andes (15°–27°S). The model predicts the observed deformation pattern of extension in the forearc, compression in the Western Monocline (corresponding to magmatic activity), extension in the Altiplano, compression in the Eastern Monocline and Subandes, and no deformation in the Brazilian Shield. By comparing the calculated solutions with the large-scale tectonic observations we are able to evaluate the forces that govern the deformation in the central Andes. The approximately constant subduction velocity in the past 26 m.y. suggests that the rate of crustal shortening in the Andes has decreased with time due to the thickening of the crust.

INTRODUCTION

In recent years, studies of continental tectonics have treated the continental lithosphere as a continuum and have successfully described large-scale continental deformation [e.g., *Tapponier and Molnar*, 1976; *Bird and Piper*, 1980; *England and McKenzie*, 1982, 1983; *Vilotte et al.*, 1982, 1986]. Some studies assumed that the continental lithosphere overlies an inviscid asthenosphere [e.g., *England and McKenzie*, 1982, 1983; *Houseman and England*, 1986] or have imposed shear tractions at the base of the lithosphere [e.g., *Bird and Baumgardner*, 1984] and investigated the deformation independent of asthenospheric flow. Similarly, studies of mantle convection either ignored the overlying lithosphere [e.g., *McKenzie et al.*, 1973] or assumed a rigid lithosphere [e.g., *Hager and O'Connell*, 1981] and studied mantle flow independent of lithospheric deformation. (Because the asthenosphere refers to a small part of the mantle, some studies prefer to use the term mantle, rather than asthenosphere, to describe the region beneath the lithosphere.) Independent studies of the two systems (continental lithosphere and asthenosphere) are reasonable as long as the interaction between the two is limited. When continental deformation and asthenospheric flow strongly influence each other, one must consider the two systems together.

Continental lithosphere overlying a subduction zone is an environment of major interaction between continental lithosphere and asthenospheric flow. Previously, *Wdowinski et al.* [1989] treated the problem as a superposition of two linear models: a thin viscous sheet model to calculate the deformation of the overlying continental lithosphere and a corner flow model to calculate the asthenospheric flow underneath. In this study we take a somewhat different approach, and investigate the lithosphere and the asthenosphere as a single system by using a plane strain flow model of the upper 700 km of the Earth. Furthermore, we use numerical methods, which enable us to investigate more complex and perhaps realistic models.

The Andes presents the best example of a mountain belt overlying a subduction zone, and is the type locality of active plate boundaries (Andean-type), which represent a tectonic environment of compressional deformation and mountain building above a subduction zone. Many studies have used the present-day Andean topography and tectonics as a possible analog of mountain building processes above subduction zones in the past (e.g., the Laramide Orogeny in the western United States during Late Cretaceous and Early Tertiary time [*Hamilton*, 1969; *Burchfiel and Davis*, 1975]). The present-day tectonic activity in the central Andes (15°–27°S) exhibits regions of large-scale compression and extension and of magmatic activity that are continuous along strike of the mountain belt (Figure 1). Surface extension is found in the forearc region near the trench and in the high Altiplano plateau; however, there are no constraints to indicate whether the deformation at deeper levels is extensional as well. Compression is found in the eastern part of the Andes, about 600–900 km east of the trench.

The high topography of the Andes is supported by a thick crust [*James*, 1971] and possibly by a thermally thinned lithosphere underlain by low-density asthenosphere [*Froidevaux and Isacks*, 1984]. The extension in the forearc region has been explained by tectonic erosion, that is, shearing and undercutting of the overriding plate by the subducting slab [*Karig*, 1974; *Coulbourn*, 1981]. The extensional deformation in regions of high topography is attributed to excess vertical stress under high mountains [*Dalmayrac and Molnar*, 1981]; whereas the compression at the eastern flanks of the Andes is attributed to horizontal shortening in the E-W direction caused by underthrusting of the Brazilian Shield westward [*Suárez et al.*, 1983; *Isacks*, 1988]. The close proximity of extensional and compressional stress regimes at the edge of the Altiplano has been explained by combined effect of tectonic and buoyancy forces [*Froidevaux and Isacks*, 1984; *Molnar and Lyon-Caen*, 1988].

[1]Now at Scripps Institution of Oceanography, La Jolla, California.

Copyright 1991 by the American Geophysical Union.

Paper number 91JB01196.
0148-0227/91/91JB-01196$05.00

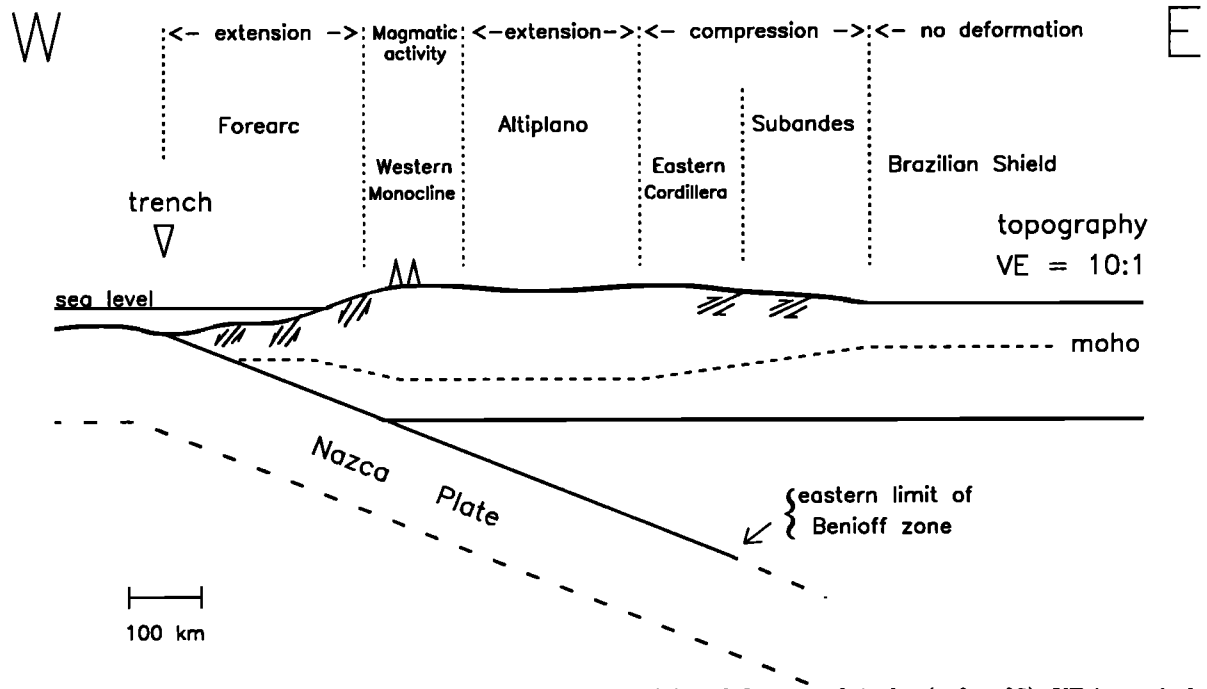

Fig. 1. Schematic cross section showing the tectonic activity of the central Andes (15°–27°S). VE is vertical exaggeration.

In this study we investigate quantitatively the effects of tectonic and buoyancy forces on the deformation of the entire Andean region, by using a plane strain flow model of the Nazca–South America subduction zone. In order to keep the model simple, we consider only the mechanical and neglect the thermal aspects of the deformation. As a result the model may be less applicable to regions where thermal processes play an important role, such as in the magmatically active Western Monocline. Elsewhere, where the deformation is dominated by mechanical processes, the model can explain many aspects of the complex Andean tectonics that have heretofore not been explained by other models.

MODEL

Our region of interest is the continental lithosphere overriding a subduction zone, between the trench and the end of the subducting slab (Figure 2). However, a larger region is considered, because the overriding continental lithosphere, the subducting oceanic lithosphere, and the asthenosphere are dynamically interactive. The flow in the asthenosphere that affects the deformation within the overlying lithosphere is predominantly driven by the subducting slab and is confined to the upper mantle. The flow in the lower mantle, whether or not flow penetrates the 670 km discontinuity, has little influence on the deformation of the overlying continental lithosphere and hence is omitted from our calculations.

We consider a simple model of a subduction zone comprised of continental lithosphere (composed of crust and mantle), subducting oceanic lithosphere, and asthenosphere. In the model, the continental lithosphere is strong, the asthenosphere is weak, and the strength of the subducting slab varies in different computations, from very strong (rigid) to as weak as the asthenosphere. In order to keep the model simple, the strength for the continental lithosphere is assumed to be uniform even though it is comprised of crust and

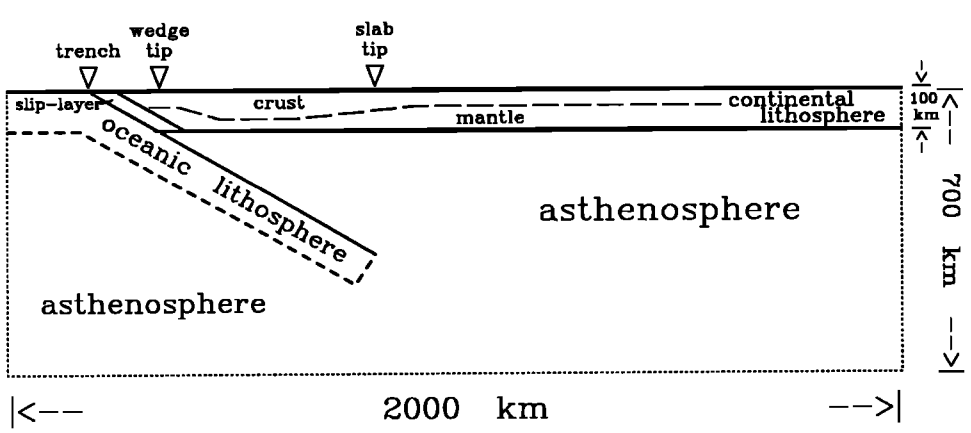

Fig. 2. Schematic diagram of the model showing the subduction zone geometry based on the Nazca–South America Benioff zone in the segment 15°–27°S. The geometry of the subducting slab (planar with 30° dip) is defined from seismic activity in the Benioff zone. The crustal thickness is derived from the Andean topography, which is assumed to be isostatically supported (long-dashed lines). A slip layer of finite thickness (exaggerated here) accommodates most of the deformation between the subducting slab and the overriding continental lithosphere.

mantle. The contact between the continental lithosphere and the descending subducting slab is a narrow zone of intense shearing and heat generation by viscous dissipation [*Turcotte and Oxburgh*, 1968; *Jischke*, 1975]. As a result, the strength of this region is significantly weaker than that of the continental lithosphere or of the subducting oceanic lithosphere. Correspondingly, we define a very weak slip layer that accommodates most of the shear deformation between the subducting oceanic lithosphere and the overlying continental lithosphere.

The geometry of the subducting slab and the crustal thickness are important parameters that affect the deformation in the overriding continental lithosphere [*Wdowinski et al.*, 1989]. In order to minimize the number of free parameters in the model, we use the geometry of the Nazca–South America subduction zone and the Andean crustal structure in the region between 15°S and 27°S. Seismic studies of the Benioff zone indicate that the Nazca plate is being subducted beneath this segment at an angle of 30° for a horizontal distance of about 700 km east of the trench [*Stauder*, 1975; *Barazangi and Isacks*, 1976]. The Andean topography, as any other large extensive topographic feature, is compensated by low-density mass at depth. We use the observed topography, the principle of isostasy, and assume uniform crustal and mantle densities to derive a simple crustal structure that is shown in Figure 2. Other crustal structures, which can be derived by assuming a more complicated density structure, such as low density asthenospheric root beneath the Altiplano [*Froidevaux and Isacks*, 1984], are not considered in this study.

Mathematical Formulation

The continental lithosphere and the asthenosphere are assumed to behave over long time intervals as incompressible viscous fluids. The lateral extent of the Nazca–South America subduction zone allows us to neglect along strike variations and to use two-dimensional plane strain calculations (the flow is everywhere parallel to the xz plane and is independent of the y axis ($u_y = 0$)). There are three sets of equations that govern the two dimensional flow. First, the force balance equation

$$\nabla \cdot (\tau - Ip) = \rho g \mathbf{a} \tag{1}$$

where τ is the deviatoric stress tensor, I is the second rank identity tensor, p is the pressure, ρ is the density, g is the acceleration due to gravity, and $\mathbf{a}$ is the vertical unit vector. Second, the continuity equation for an incompressible material

$$\nabla \cdot \mathbf{u} = 0 \tag{2}$$

where $\mathbf{u}$ is the velocity. Finally, linear constitutive relations

$$\tau = 2\eta\dot{\epsilon} \tag{3}$$

where τ is the deviatoric stress tensor, η is the viscosity, and $\dot{\epsilon}$ is the strain rate tensor ($\dot{\epsilon}_{ij} = \frac{1}{2}(u_{i,j} + u_{j,i})$). These equations yield the following dimensionless governing equation:

$$\eta\nabla^2\mathbf{u} - \nabla p = \rho a Gr \tag{4}$$

where Gr is the Grashof number

$$Gr = \frac{g\rho_0 x_0^2}{\eta_0 u_0} \tag{5}$$

x_0, u_0, η_0, and ρ_0 are the characteristic length, velocity, viscosity, and density, respectively. The dimensionless strain rate $\dot{\epsilon}$ is scaled by u_0/x_0 and the dimensionless pressure p is scaled by $x_0/\eta_0 u_0$. The Grashof number represents the ratio of buoyant to viscous forces [*Turner*, 1973]. Zero Grashof number ($Gr = 0$) indicates that buoyancy forces are negligible, while infinite Grashof number ($Gr \to \infty$) represents a flow that is dominated by buoyancy forces. In this study, the characteristic length, velocity, and density are fixed; thus the Grashof number is sensitive only to the characteristic viscosity. The characteristic parameters (Table 1) yield values of the Grashof number in the range 0.1–10.

TABLE 1. Values of the Characteristic Parameters That Are Used to Evaluate the Grashof Number in Calculations

	Parameter	value
g	gravitational acceleration	10 m s^{-2}
x_0	characteristic length	100 km
u_0	characteristic velocity	100 mm yr^{-1}
ρ_0	characteristic density	3270 kg m^{-3}
η_0	characteristic viscosity	10^{22}–10^{24} Pa s
Gr	Grashof number	0.1–10

The governing equation (4) is solved numerically via a finite element method by using 200–500 (in various numerical experiments) 8-noded quadrilateral isoparametric elements. We solve for the velocity field by using a penalty function and selective reduced integration technique [*Zienkiewicz*, 1977]. Various patch tests have been conducted to ensure that our code is free of zero-energy and propagating spurious modes [*Zienkiewicz*, 1988].

Parameter Ranges

The strengths of the continental lithosphere, the asthenosphere, and the slip layer are represented by their effective viscosities, which are specified a priori (Figure 3). Studies of asthenospheric viscosity from postglacial rebound, assuming a linear rheology, yield an average asthenospheric viscosity η_a of $\sim 10^{21}$ Pa s [*Cathles*, 1975; *Peltier and Andrews*, 1976]. The effective viscosity of oceanic and continental (shield) lithosphere is 10^{23}–10^{24} Pa s, estimated from the flexural response to long-term loads [*Walcott*, 1970]. However, actively deforming continental lithosphere may have a lower effective viscosity, of the order of 10^{22} Pa s [*Wdowinski et al.*, 1989]. *Jischke* [1975] has estimated the slip layer viscosity η_{sl} to be 10^{20}–10^{21} Pa s. We choose the lithospheric viscosity η_l as the characteristic viscosity ($\eta_0 = 10^{22}$–10^{24} Pa s). The density structure that determines the pressure gradients induced by the buoyancy forces must be specified as well. We consider a simple case of a buoyant crust overlying a heavier mantle; the crustal density ρ_c is assumed to be 15% less then the mantle density ρ_m (2780 kg m^{-3} versus 3270 kg m^{-3}).

The ability of the asthenospheric flow to influence the deformation within the lithosphere is determined by the viscous coupling between the asthenosphere and the lithosphere (η_a/η_l) and the thickness of the lithosphere (L). The ratio of these two parameters is defined as the asthenospheric parameter ($\zeta_a = \eta_a/\eta_l L$), which is similar to the small parameter of the perturbation solution that was used by *Wdowinski et al.* [1989]. Similarly, the slip layer param-

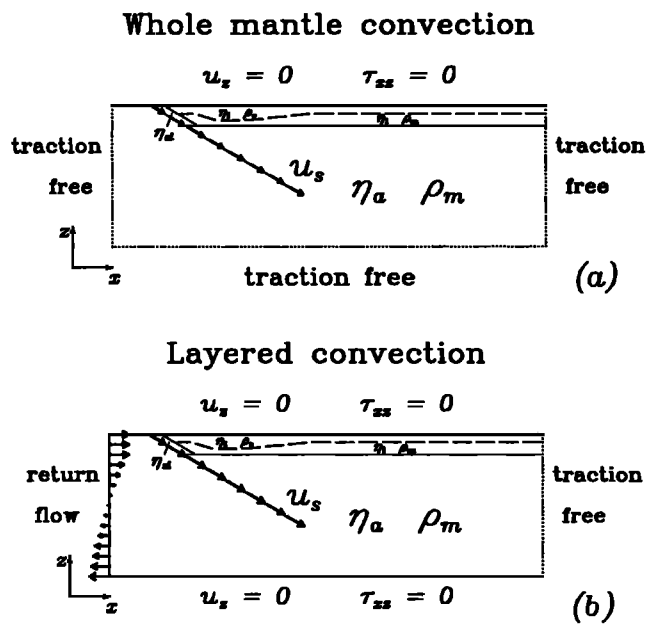

Fig. 3. Schematic diagram of the model showing the parameters and boundary conditions of the flow within the subduction zone for (*a*) whole mantle convection and (*b*) layered mantle convection with the parameters η_l, lithospheric viscosity; η_a, asthenospheric viscosity; η_{sl}, slip layer viscosity; ρ_c, crustal density; ρ_m, mantle density; u_s, subduction velocity; u_z, vertical velocity; and τ_{xz}; the shear component of the stress tensor.

eter, which determines the ability of the slip layer to affect the lithospheric deformation, is defined as $(\zeta_{sl} = \eta_{sl}/\eta_l S_{sl})$; where (η_a/η_l) is the viscous coupling between the slip layer and the lithosphere and S_{sl} is the thickness of the slip layer. Using the above viscosity estimates and the dimensionless thicknesses of the lithospheric and the slip layer (Table 2), we estimate the asthenospheric and the slip layer parameters to be in the range 10^{-1}–10^{-3}.

TABLE 2. Values of the Dimensionless Parameters Used in the Calculations

	Parameter	value
L	lithospheric thickness	1.00
S_0	normal crustal thickness	0.35
S_1	thick crustal thickness	0.60
S_{sl}	slip-layer thickness	0.01–0.10
θ_0	angle of subduction	30°
ζa	asthenospheric parameter	10^{-1}–10^{-3}
ζsl	slip layer parameter	10^{-1}–10^{-3}
ρc	crustal density	0.85
ρm	mantle density	1.0

Boundary Conditions

The upper and lower boundaries represent natural boundaries in the Earth that can impose some constraints of the flow. The upper boundary is fixed at sea level ($z = 0$), which represents the Earth's surface without topography, and the lower boundary is fixed at depth of 700 km, which represents the boundary between the upper and lower mantle. The vertical boundaries of the model, however, are chosen arbitrarily because, at the regional scale of the problem (1000–2000 km), there are no natural vertical boundaries that can impose any constraints on the flow. In order to minimize the effects of these arbitrary boundaries, their horizontal locations are chosen to be significantly far from our region of interest, the deformed part of the continental lithosphere between the trench and the slab tip.

Two types of boundary conditions (Figure 3), which correspond to whether or not the flow penetrates the 670 km discontinuity, are considered. These are referred to as either whole mantle convection or layered mantle convection. In either case, the boundary conditions along the upper surface and the subducting slab are identical. We impose zero vertical motion ($u_z = 0$) and zero shear traction ($\tau_{xz} = 0$) along the upper boundary, the location of which is fixed at sea level ($z = 0$). In reality, the Earth's surface moves vertically and generates surface topography (up to 5 km of relief). Nevertheless, the vertical velocity of the Earth's surface is very small (< 1 mm yr^{-1}) and hence negligible at the velocity scale of the problem (100 mm yr^{-1}). The advantage of zero vertical velocity ($u_z = 0$) boundary conditions is that they allow us to investigate the effects of the tectonic forces independent of the buoyancy forces (see below). The vertical component of the tectonic forces (subduction), which in reality is balanced by buoyancy forces, is balanced in this case by surface forces along the upper boundary. The disadvantage of these boundary conditions is that they are less applicable to the region close to trench, where the trench topography and tectonics are dominated by the vertical component of the subduction [*Wdowinski and O'Connell*, 1990].

The subduction of the oceanic lithosphere is introduced through velocity boundary conditions along the upper surface of the subducting slab. In reality the subducting slab has a finite thickness, which is not considered in this model because the deformation within the overriding lithosphere is not sensitive to the flow below the upper surface of the slab. A constant subduction velocity u_s represents rigid slab subduction, while variations in the subduction velocity along the slab represent slab deformation.

In the case of whole mantle convection (Figure 3*a*), the flow can pass through the bottom boundary, which in this case does not introduce any constraints on the flow. Thus a traction free condition ($\tau_{zz} = \tau_{xz} = 0$) and lithostatic pressure ($p = \int \rho g dz$) may be imposed as boundary conditions. Similarly, a traction free condition ($\tau_{xx} = \tau_{xz} = 0$) and lithostatic pressure are imposed on the vertical side boundaries, because they are not natural boundaries and the flow can penetrate through them. These boundary conditions allow these arbitrarily chosen boundaries (dotted lines in Figure 3*a*) to deform according to the flow within the asthenosphere and the lithosphere. In the case of layered mantle convection (Figure 3*b*), the flow is restricted to the upper 700 km of the Earth and cannot penetrate the lower boundary ($u_z = 0$). Thus we impose zero shear traction ($\tau_{xz} = 0$), which allows horizontal flow along this boundary. Along the right vertical boundary a traction free condition is imposed, as in the case of whole mantle convection. Global flow models [e.g., *Hager and O'Connell*, 1979] indicate that the strong upwelling beneath the East Pacific Rise generates a closed circulation flow pattern between the subducting Nazca plate and the nearby ridge. Therefore we impose a return flow, that is a velocity boundary condition that conserves the mass of flow, along the left vertical boundary. In layered mantle convection, all the flow that enters in the upper part of asthenosphere (100–300 km depth) with the subducting slab returns

to the ridge nearby by flow in the lower part of the asthenosphere (400–700 km depth). In the case of whole mantle convection, the flow can return to the ridge at depths much greater than 700 km, and it is not necessary to impose a return flow condition.

Results

Figure 4 shows the calculated velocity field for the whole mantle convection and layered mantle convection boundary conditions with subduction of a rigid slab ($u_s = 1$), and the parameters $u_s = 1.0$, $\zeta_a = 5 \times 10^{-3}$, and $\zeta_{sl} = 10^{-2}$. Although the patterns of flow in the lower levels of the asthenosphere are different for the two cases, the flow patterns within the lithosphere and in the upper levels of the asthenosphere are very similar. Basically, the flow follows the wedge shape of the subduction zone, which confirms simple corner flow calculations of flow within a subduction zone [e.g., *Wdowinski et al.*, 1989]. The flow field within the continental lithosphere (Figures 4*c* and 4*d*) is predominantly horizontal with negligible shear. This allows us to characterize the flow within the lithosphere by the vertically averaged horizontal velocity u_x and the vertically averaged horizontal strain rate $\dot{\epsilon}_{xx}$. Because numerical solutions are used, the vertically averaged velocities and strain rates are not necessarily smooth functions. The average rate of lithospheric thickening or thinning is proportional to the average vertical strain rate $\dot{\epsilon}_{zz}$. Using the incompressible condition ($\dot{\epsilon}_{xx} = -\dot{\epsilon}_{zz}$), we can describe the state of lithospheric deformation as a function of the average horizontal strain rate $\dot{\epsilon}_{xx}$. Lithospheric compression occurs when $\dot{\epsilon}_{xx} < 0$, and extension occurs when $\dot{\epsilon}_{xx} > 0$. The flow in the region adjacent to the wedge tip changes significantly with depth; hence the vertically averaged representation of the flow is less accurate in this area.

Figure 4 shows that the flow fields within the overriding continental lithosphere are almost identical for the two types of boundary conditions. Thus, to eliminate redundancy, we choose to present only results that are calculated with whole mantle convection boundary conditions. The two types of forces that dominate the deformation within the overriding continental lithosphere are tectonic forces due to the subduction of oceanic lithosphere and buoyancy forces due to variations in crustal thickness. Because a linear rheology is used, one can investigate separately the effect of each of the two types of forces on the overall flow with an emphasis on the deformation within the overriding continental lithosphere as shown by the vertically averaged strain rate. Figure 5 shows the parameters and boundary conditions used to calculate the two separate flow fields generated by the tectonic forces and by the buoyancy forces. The flow field solutions for the two sets of boundary conditions (Figure 6) have similar wedge-shaped flow patterns but are in opposite directions. We investigate the effects of the two forces and their combined effect on the deformation within the overrid-

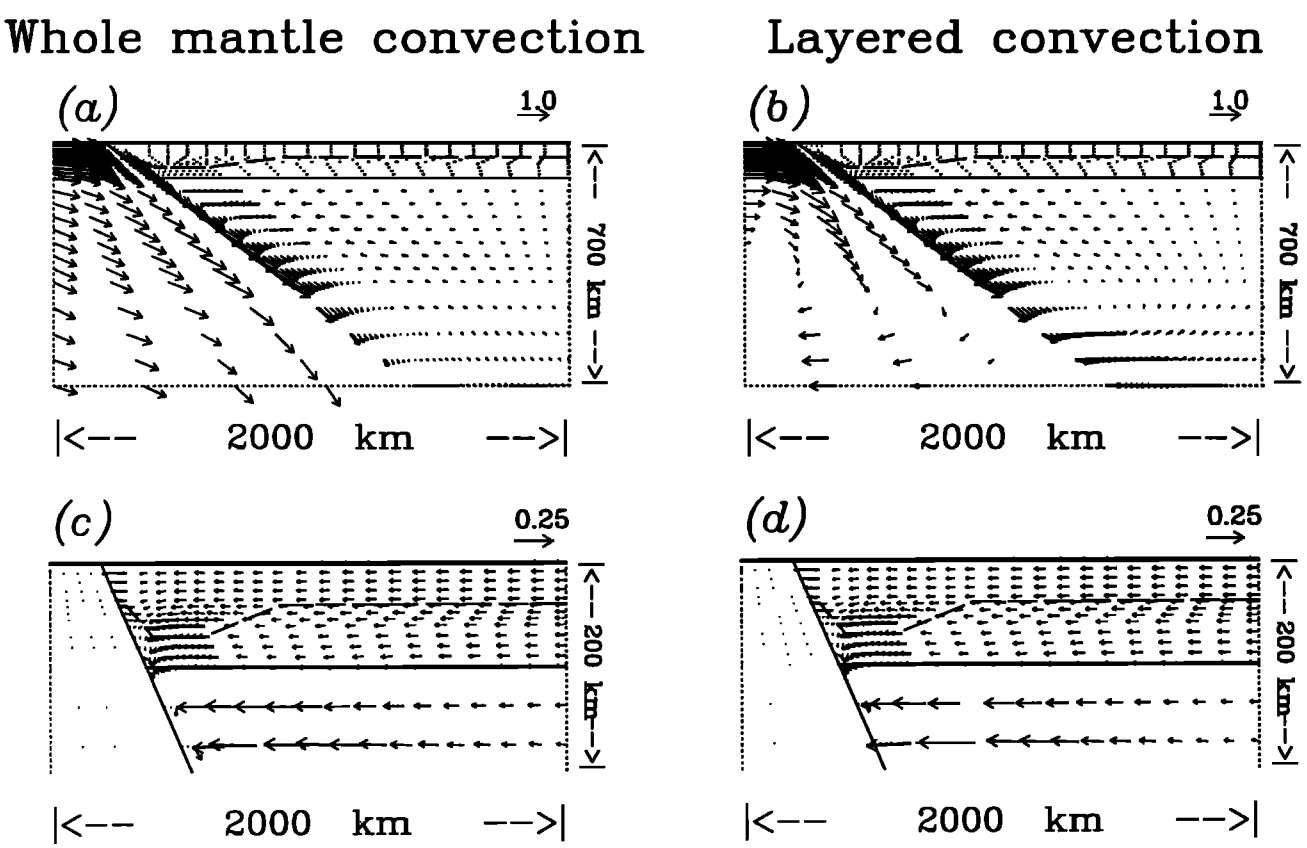

Fig. 4. Velocity solutions for subduction of a rigid plate for (*a* and *c*) whole mantle convection and (*b* and *d*) layered mantle convection with the parameters $u_s = 1.0$, $\zeta_a = 5 \times 10^{-3}$, $\zeta_{sl} = 10^{-2}$, and $Gr = 5$. The flow field in the upper 700 km of the Earth follows the wedge shape of the subduction zone (Figures 4*a* and 4*b*). The velocity field in the upper 200 km, as magnified to see the low-magnitude lithospheric flow, is dominated by horizontal flow and is very similar for both types of mantle convection (Figures 4*c* and 4*d*).

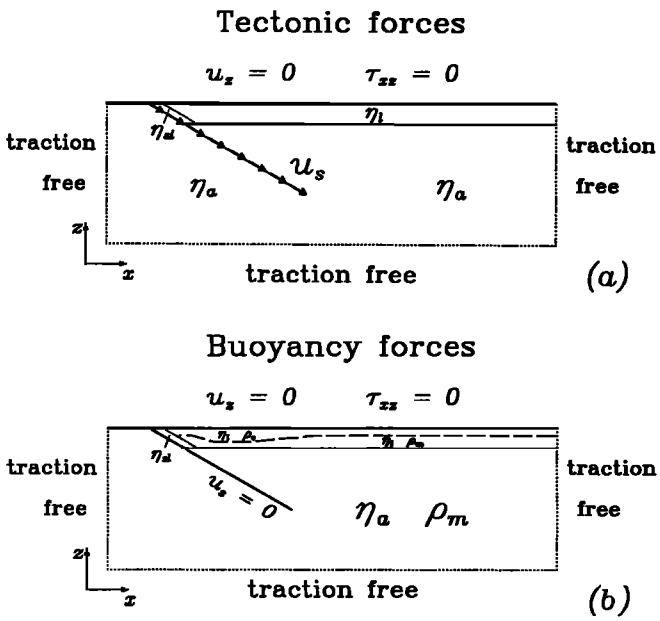

Fig. 5. Schematic diagram of the model showing the parameters and boundary conditions used to investigate the effect of (*a*) tectonic forces and (*b*) buoyancy forces on the flow. The parameters are the same as in Figure 3.

ing continental lithosphere by using the vertically averaged representation.

Figures 7*a* and 7*c* show the vertically averaged velocity and strain rate fields within continental lithosphere that is subjected only to tectonic forces ($u_s = 1$; $Gr = 0$). Near the trench the subducting slab shears the base of the lithosphere along the slip layer and generates extension, which is sensitive to ζ_{sl}. The averaged strain rate curve near the trench (Figure 7*c*) is not smooth because the vertically averaged representation is not very accurate in that region. A more careful analysis of the near-trench deformation shows that the extension (tectonic erosion) near the trench is more likely to be caused by a change of one of the model parameters rather than depends only on ζ_{sl} [*Wdowinski and O'Connell*, 1990]. Farther inland, the continental lithosphere overlies the asthenosphere. The flow in the asthenosphere, which follows the subducting slab, shears the base of the lithosphere toward the trench, causing the continental lithosphere to move in the same direction. The magnitude of the velocities decreases toward the trench, which gives rise to increasing compressional strain rates. The strain rate curve has a spike, because the transition between the compressional and extensional regimes occurs at a short distance from the tip of the asthenospheric wedge. As shown in Figures 7*a* and 7*c*, the magnitudes of the velocity and the strain rate increase with ζ_a, which represents the viscous coupling between the asthenosphere and the lithosphere.

Figures 7*b* and 7*d* show the vertically averaged velocity and strain rate fields within continental lithosphere that is subjected only to buoyancy forces ($u_s = 0$; $Gr = 1, 5, 10$). The nonuniform crustal thickness induces a horizontal pressure gradients, which drives lithospheric flow from regions of thick crust to regions of thinner crust. The vertically averaged strain rate solution (Figure 7*d*) shows mainly ex-

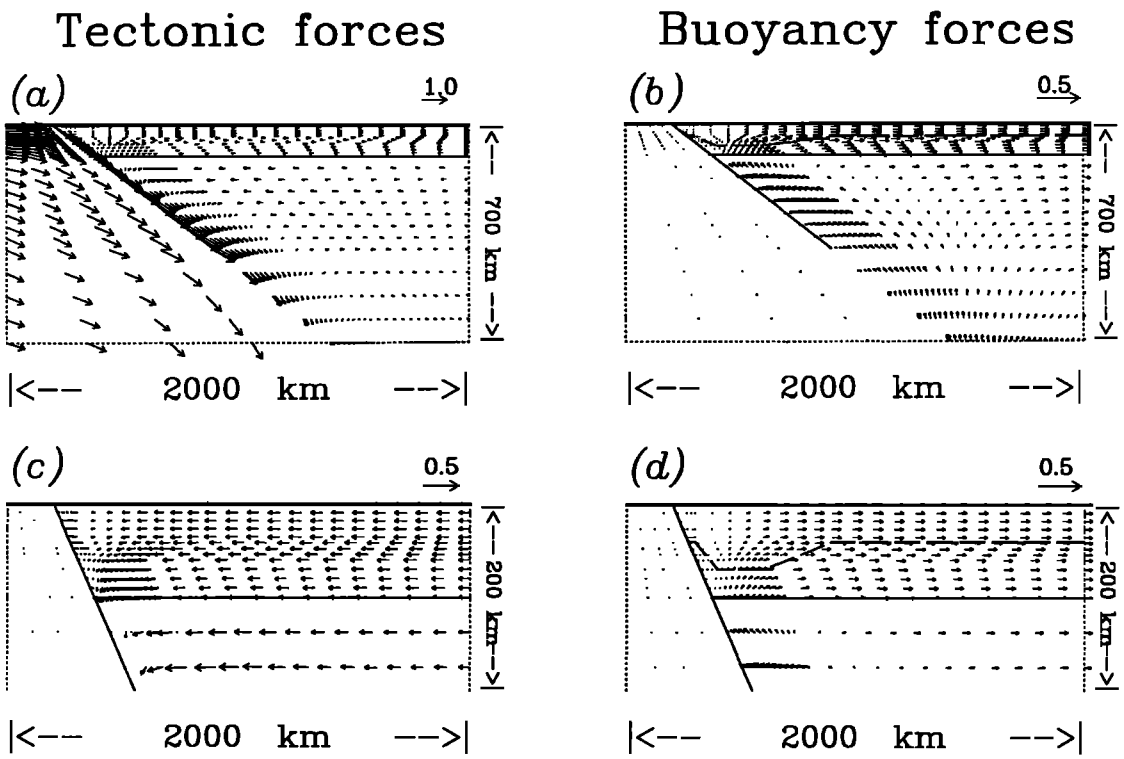

Fig. 6. Velocity solutions for (*a* and *c*) tectonic forces and (*b* and *d*) buoyancy forces with the parameters $u_s = 1.0$, $\zeta_a = 5 \times 10^{-3}$, $\zeta_{sl} = 10^{-2}$, and $Gr = 5$. For the tectonic forces, $u_s = 1.0$ and $Gr = 0$ (Figures 6*a* and 6*c*), and for the buoyancy forces, $u_s = 0.0$ and $Gr = 5$ (Figures 6*b* and 6*d*). The flow field in the upper 700 km of the Earth follows the wedge shape of the subduction zone but acts in opposite directions in Figures 6*a* and 6*b*. The velocity field in the upper 200 km, as magnified to see the low-magnitude lithospheric velocity, is dominated by horizontal flow (Figures 6*c* and 6*d*).

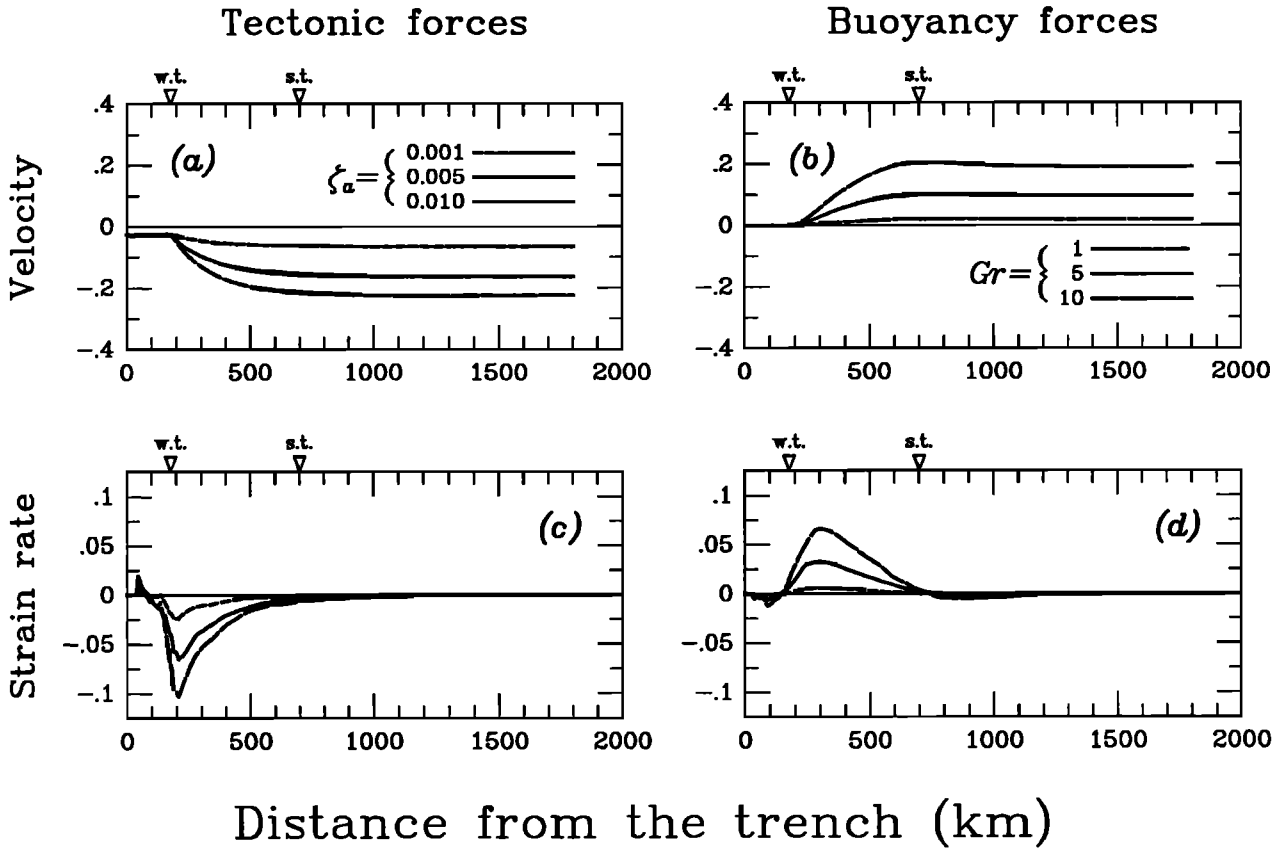

Fig. 7. Vertically averaged velocity and strain rate solutions for (a and c) the tectonic forces and (b and d) the buoyancy forces. The tectonic forces are sensitive to the asthenospheric parameter ζ_a, and the buoyancy forces to the Grashof number Gr. The velocity is scaled by the characteristic velocity u_0, and the strain rate is scaled by u_0/x_0. The location of the wedge tip and the slab tip are indicated by w.t. and s.t., respectively.

tensional deformation along the thickened crust and minor compression at the edges of the thickened crust. Inasmuch as the trench location is fixed (through the boundary conditions), the thick crust can extend only inland. The magnitudes of the velocity and of the extensional strain rate are proportional to the Grashof number, which represents the ratio of buoyancy forces to viscous forces. Because the density variations are confined to the lithosphere, the role of the Grashof number Gr in our model is similar to that of the Argand number Ar in the thin viscous sheet model of *England and McKenzie* [1982].

The seismic activity within Benioff zones indicates some deformation within the subducting slab. *Isacks and Molnar* [1971] showed that at shallow depth subducting slabs are usually under extension in a direction parallel to the slab dip, whereas at greater depth they are under compression parallel to the slab dip. The rate of deformation within the subducting slab can be as large as a few times 10^{-15} s^{-1} [*Giardini and Woodhouse*, 1986; *Bevis*, 1988]. Figure 8 shows the effect of various rates of slab extension on the overriding continental lithosphere. An increase in the magnitude of slab extension tends to increase the magnitude of the compression in the overriding plate, with a minor effect on the distribution of strain rates, and has an effect similar to that of increasing asthenospheric parameter ζ_a. We also investigate the influence of the length of the subducting slab on lithospheric deformation. Our results shows that the overall flow pattern, which follows the wedge shape of the subduction zone, is not sensitive to the length of the slab as long as the slab is longer than 400 km. As a result, the deformation within the overriding continental lithosphere (constrained by observations) is not sensitive to changes in this parameter. The sensitivity of the solution to other geometrical parameters, such as the angle of subduction or the thickness of the lithosphere, were studied by *Wdowinski et al.* [1989] and are not investigated in this study.

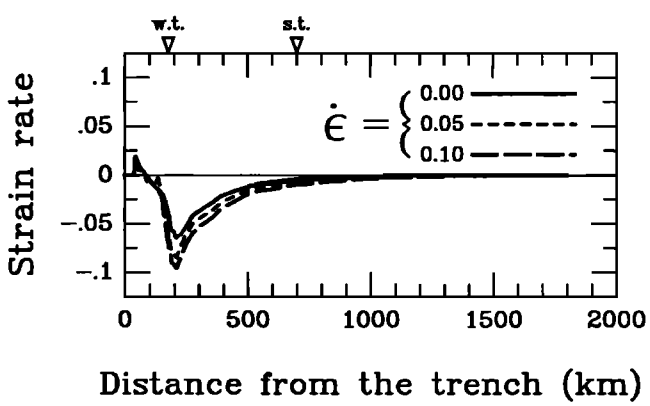

Fig. 8. Vertically averaged strain rate solutions showing the sensitivity of the tectonic forces to extension within the subducting slab. The strain rate is scaled by u_0/x_0. The location of the wedge tip and the slab tip are indicated by w.t. and s.t., respectively.

TECTONIC ACTIVITY IN THE CENTRAL ANDES

Observations

The topography of the central Andes between 15°S and 27°S is characterized by a broad intermontane plateau (> 400 km wide) of elevation exceeding 3 km. The topography is supported by a thick crust with an average thickness of 60 km [*James*, 1971]. The tectonic activity, however, extends over a region up to 900 km wide from the trench in the west to the Subandes in the east (Figure 1). Although the Andean mountain belt represents a tectonic environment of compression and mountain building above a subduction zone, broad zones of extensional tectonism are located in the forearc region and in the Altiplano. Interestingly, the eastern limit of the Benioff zone seismicity coincides with the eastern limit of the deformation in the overriding South American plate [*Jordan et al.*, 1983].

The extensive normal faults observed in the forearc region, mostly below sea level, represent an extensional tectonic environment [*Kulm et al.*, 1981; *von Huene et al.*, 1988]. Active normal faults are also observed inland, along the Pacific coast [*Sébrier et al.*, 1985]. The Western Monocline (Cordillera Occidental) is a region of magmatic activity and is covered by recent volcanic flows. There are no surface observations, nor seismic activity, to indicate whether this region is currently under compression or extension. Farther inland, the Altiplano overlies a thick continental crust. Although the crust had presumably thickened under a compressional stress regime, at present the northern and southern parts of the plateau are extending by normal and strike-slip faults [*Suárez et al.*, 1983; *Sébrier et al.*, 1985]. It is not clear whether the observed extension in the northern and southern sections of the Altiplano represents the state of deformation throughout the entire Altiplano lithosphere, especially if we consider the lack of observations in deeper levels of the lithosphere. Compressional tectonic activity is observed in the eastern part of the mountain belt, in the Eastern Cordillera (Cordillera Oriental) and in the Subandes. The seismic activity is concentrated in a narrower region, along the eastern flanks of the mountain belt in the Subandes [*Suárez et al.*, 1983]. East of the Subandes, in the Brazilian Shield, no large-scale deformation or significant seismic activity is observed.

Model Results

Many aspects of the complex tectonic environment of the Andes can be explained by the combined effects of tectonic and buoyancy forces. The tectonic forces, which arise from the subduction of oceanic lithosphere, cause minor extension near the trench and compression farther inland (Figure 7*c*). The buoyancy forces, which arise from relaxation of overthickened crust, extend the lithosphere in regions of thick crust and cause minor compression near the edges of the thickened crust region (Figure 7*d*). The distribution of the combined deformation depends on the choice of parameters and velocity boundary conditions, which are shown in Table 1 and Table 2.

Figure 9 shows a solution with the parameters $\zeta_a = 3 \times 10^{-3}$, $\zeta_{sl} = 10^{-2}$, and $Gr = 3$ that best matches the observations. The vertically averaged strain rate field of the overriding lithosphere shows five distinct provinces, which can be correlated with the observations (Figure 1). The

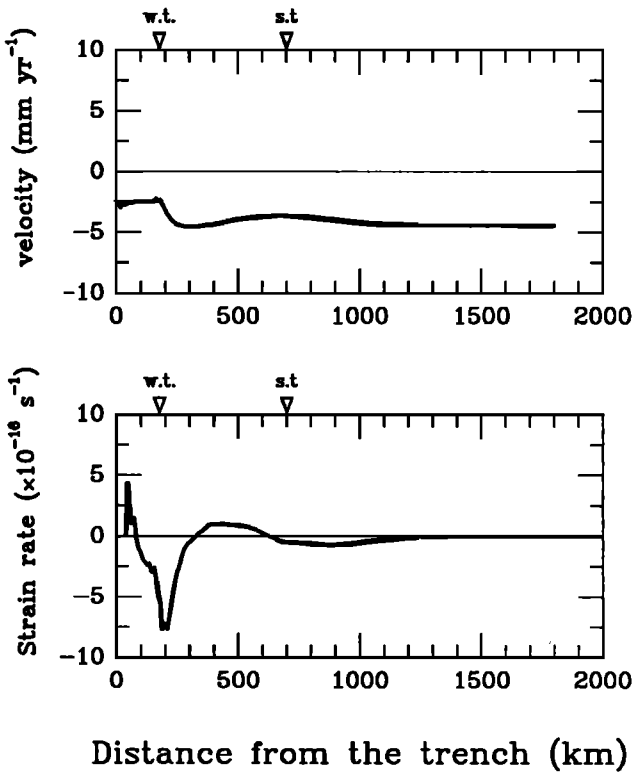

Fig. 9. A combined solution for the tectonic and buoyancy forces ($u_s = 1.0$, $\zeta_a = 3 \times 10^{-3}$, $\zeta_{sl} = 1 \times 10^{-2}$, and $Gr = 3$). The location of the wedge tip and the slab tip are indicated by w.t. and s.t., respectively. The vertically averaged strain rate solution shows five distinct provinces of extensional and compressional deformation, which are in a good agreement with the observations from the Andes (Figure 1).

characteristics of the five provinces are extension in the forearc, compression in the Western Monocline, extension in the Altiplano, compression in the Eastern Cordillera and Subandes, and no deformation in the Brazilian Shield. The low magnitude of the calculated strain rate (of the order of 10^{-16} s^{-1}) is in good agreement with the seismic strain rate in the Subandes [*Suárez et al.*, 1983]. The calculated extensional strain rates for the Altiplano (Figure 9) are comparable in magnitude to the compressional strain rates in the Subandes. This may be an overestimate of the extensional strain rates in the Altiplano, which are not well constrained, but it demonstrates well the phenomena of extensional deformation in regions of thick continental crust. A similar deformation pattern is obtained when extension within the subducting slab is included. As shown in Figure 9, slab extension of the order 3×10^{-15} s^{-1} with $\zeta_a = 2 \times 10^{-3}$ and $Gr = 3$ generates a vertically averaged strain rate curve that is very similar to that for rigid slab subduction.

The largest discrepancy between the observations and the model's predictions occurs in the Western Monocline, where the observations of magmatic activity do not indicate any particular deformation, whereas the model predicts major compression. Because our model does not account for thermal processes, such a discrepancy might be expected. However, the magmatic activity and the major compression may be related if the magmatic activity represents redistribution of the crustal material due to compression and crustal thickening. Indeed, geochemical studies of volcanic rocks from the Western Monocline show a strong crustal signa-

ture, suggesting that a significant portion of the magma was generated within the crust [e.g., *Thrope et al.*, 1981].

Limitations of the Model

The simple model we have presented used a linear rheology; as a result, temperature variations and nonlinearities in rheology that can affect the deformation have been ignored. The temperature mostly affects the strength of rocks. The first-order effect of temperature is in fact included by separating the upper 700 km of the Earth into a strong lithosphere, a weak asthenosphere, and a very weak slip layer. Second-order temperature variations may perturb the lithospheric-asthenospheric boundary and may induce smaller-scale deformation patterns. The magmatic activity in the Western Monocline indicates that such a perturbation occurs beneath that region, and indeed the model fails to explain the observations there. Elsewhere, the length scale of such perturbations are probably smaller than the length scale of the observation (100–200 km) and therefore should not significantly affect the results of the model.

Other studies of continental deformation have recognized the importance of nonlinear rheology in calculating the deformation [e.g., *Bird and Piper*, 1980; *England and McKenzie*, 1982]. These studies assumed that the rate of continental deformation is controlled by the very strong mantle lithosphere, which deforms by power law creep. When the continental crust is very thick, as in the Andes, the average strength of the lithosphere decreases because a significant portion of the mantle lithosphere is replaced by a weak crust. The strength of the lithosphere is determined in this case by the strong upper crust, which deforms by various deformation mechanisms (e.g., brittle failure, power law creep, cataclastic flow). Thus the viscous flow assumption is intended not to represent the actual deformation mechanism but rather to relate the rate of deformation to the stress by the effective viscosity. The average strength of the lithosphere, which is represented by the effective viscosity, takes into account the response of the lithosphere to the various deformation mechanisms, including the effect of the nonlinear rheology (power law creep). In regions of very high stresses, the effect of nonlinear rheology needs to be considered, as we attempt to do by defining a slip layer of reduced viscosity; nevertheless, calculations with nonlinear rheology may produce somewhat different results.

DISCUSSION

In this study, the interaction between the lithosphere (plate) and the asthenosphere is investigated as a single system, and as a result, one can evaluate the forces that act on the base of the lithosphere. Between the trench and the tip of the asthenospheric wedge (Figure 10), the subducting slab shears the base of the continental lithosphere along the slip layer toward the wedge tip. Farther inland the continental lithosphere overrides the asthenosphere, which shears the base of the lithosphere toward the trench. The deformation that arises from these forces is minor extension near the trench and above the subducting slab, and compression farther inland, above the asthenosphere (Figure 7*c*). This contradicts previous suggestions [e.g., *Uyeda and Kanamori*, 1979], suggesting that compression in the overriding plate is a result of strong coupling between the subducting and the overlying plates. We suggest that the compression in the overriding plate arises from shear tractions acting on the base of the lithosphere toward the tip of the asthenospheric wedge from both directions.

Recent geological studies suggest that the Andean crust has been thickened during the past 15–25 m.y. by 150–250 km of horizontal shortening [*Sheffels et al.*, 1986; *Sheffels*, 1990; *Isacks*, 1988]. Thus the average shortening rate for the past 15–25 m.y. is about 10 mm yr^{-1}. However, the rate of shortening derived from seismic activity, which is averaged over 17 years, indicates a much slower motion of 1–2 mm yr^{-1} [*Suárez et al.*, 1983]. One way to explain these differences is to assume that the present-day shortening rate is the same as that obtained from geological observations, about 10 mm yr^{-1} and that the very slow shortening rate derived from the seismic activity may be a result of short sampling time or may indicate the presence of significant aseismic deformation.

We propose a different explanation based on the relation between tectonic and buoyancy forces. The tectonic forces move the far field (the Brazilian Shield) at a constant rate toward the trench as a response to the subduction of the Nazca plate (negative velocity in Figure 7*a*). The buoyancy forces move the far field at a constant rate in the opposite direction, away from the trench, as the thick Andean crust relaxes (positive velocity in Figure 7*b*). The shortening rate of the continental lithosphere is the sum of the far-field velocities. The convergence rate between the Nazca and the South America plates has remained approximately constant for the past 26 m.y. [*Pardo-Casas and Molnar*, 1987], which suggests that there were no major changes in the tectonic forces through time. However, as the Andean crust thickened, the effect of the buoyancy forces increased. Thus the shortening rate, which is the sum of the tectonic and buoyancy far-field velocities, decayed with time. Before the crust thickened appreciably, as may have been the case 15–35 m.y. ago, only the tectonic forces drove the deformation, and the rate of shortening (far-field motion) was high, about 10–30

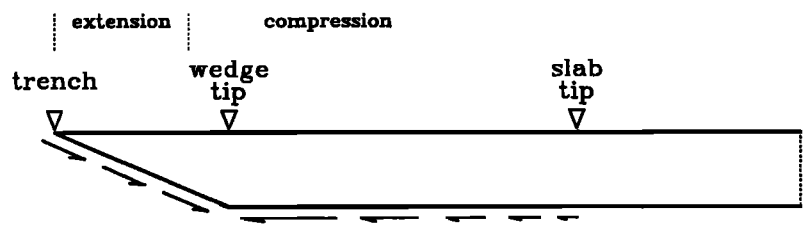

Fig. 10. A schematic illustration of the shear tractions acting on the base of the overriding continental lithosphere. Between the trench and the wedge tip the lithosphere is sheared by the subducting slab along the slip layer. Farther away, the lithosphere is being sheared by the asthenospheric flow toward the wedge tip.

mm yr^{-1}. As subduction continued, the overriding plate was shortened by the tectonic forces, and the crust thickened. The effect of the buoyancy forces increased and, as a result, the net shortening rate decreased. In order to derive the longterm average rate, the present-day shortening rate must be lower than the averaged rate (< 10 mm yr^{-1}). It may be as low as the seismically inferred strain rate, 1–2 mm yr^{-1} or higher, inasmuch as some of the deformation may be aseismic.

The model that best matches the observations (Figure 9) uses the following parameters: $Gr = 3$, $\zeta_a = 3 \times 10^{-3}$, and $\zeta_{sl} = 1 \times 10^{-2}$; however, the range of parameters that match the observation is within a factor of 2–3 of the above parameters. These values can be used to estimate the lithospheric, asthenospheric, and slip layer viscosities. The characteristic viscosity can be determined from the Grashof number because the rest of the characteristic parameters are fixed. Thus the lithospheric viscosity, which is the characteristic viscosity, is estimated to be 2–5 $\times 10^{22}$ Pa s. A different approach for estimating the effective viscosities is from consideration of the state of stress of the lithosphere. *Kanamori* [1980] estimated that the strength of the lithosphere is of the order of 100 bars. The calculated strain rates of the lithosphere are of the order of a few times 10^{-16} s^{-1} (Figure 9). The estimate of the magnitude of the stress, the calculated strain rate, and the constitutive relations (equation 3) yield an estimate of 1–5 $\times 10^{22}$ Pa s. Thus these two independent methods give similar results.

Estimates of the asthenospheric and slip layer viscosities can be derived from the asthenospheric parameter ζ_a and slip layer parameter ζ_{sl}, if the lithospheric and slip layer thicknesses are known. A lithospheric thickness of 100 km (1.0 in dimensionless units) yields an estimate of 0.5–2.5 $\times 10^{20}$ Pa s for the asthenospheric viscosity. Because the slip layer thickness is not well constrained (1–10 km), our estimate of the slip layer viscosity has a wider range of 10^{19}–10^{21} Pa s. The calculated strain rates within the slip layer are of the order of $10^{-13} - 10^{-14}$ s^{-1}. The strength of the slip layer can be estimated from the stress drop ($\sim$ 200 bars) of large subduction zone earthquakes. Again, the state of stress and the strain rates yield an independent estimate for the slip layer viscosity, which is of the order of 10^{20}–10^{21} Pa s. Our estimate of the asthenospheric viscosity (0.5–2.5 $\times 10^{20}$ Pa s) agrees with the estimate of *Wdowinski et al.* [1989], which is lower by an order of magnitude than estimates of asthenospheric viscosity (10^{21} Pa s) derived from postglacial rebound [*Cathles*, 1975; *Peltier and Andrews*, 1976], but higher by a factor of two than estimates of the viscosity of the uppermost asthenosphere (4×10^{19} Pa s) [*Cathles*, 1975]. Our estimate of the lithospheric viscosity (2–5 $\times 10^{22}$ Pa s) is higher by a factor of 2–5 than the estimate of *Wdowinski et al.* [1989]. The discrepancy between the two estimates probably arises from the consideration of buoyancy forces in the calculation of this study, which had been neglected by *Wdowinski et al.* [1989]. Our estimate of the slip layer viscosity agrees with the estimate of *Jischke* [1975] (10^{20}–10^{21} Pa s) for 1–5 km of slip layer thickness, which is thinner than the 10 km suggested by *Jischke* [1975].

CONCLUSIONS

We have presented a simple viscous flow model of subduction zones in order to calculate the deformation within the overriding continental lithosphere. The two kinds of forces that dominate the deformation within the overriding lithosphere are tectonic and buoyancy forces. Because a linear rheology is used, one is able to investigate the effect of each of these forces separately. The tectonic forces, which arise from the subduction of oceanic lithosphere, cause minor extension within the overriding lithosphere near the trench and compression farther away from the trench. The magnitude of the compression is determined by the ratio of asthenospheric to lithospheric viscosities, which represent the viscous coupling between the asthenosphere and the lithosphere, and by the rate of extension within the subducting slab. The buoyancy forces, which arise from variations in crustal thickness, cause the overriding lithosphere to extend where the crust is thick. The rate of extension is determined by the Grashof number Gr, which represents the ratio of buoyancy to viscous forces.

The model is applied to the central Andes (15°–27°S), where the deformation within the overriding continental lithosphere extends over a very wide region (up to 900 km). Benioff zone seismicity indicates that the Nazca plate is being subducted beneath this segment at an angle of 30° for a horizontal distance of about 700 km east of the trench. The tectonic activity in the central Andes presents a complex pattern of large-scale extension and large-scale compression in close proximity to one another. Our model predicts extension in the forearc, compression in the Western Monocline (corresponding to magmatic activity), extension in the Altiplano, compression in the Eastern Cordillera and Subandes, and no deformation in the Brazilian Shield. The compressional deformation observed in the Andes is a result of shear tractions acting on the base of the lithosphere toward the tip of the asthenospheric wedge from both directions. This contradicts a common explanation that the compressional tectonic environment of the Andes is a result of a strong coupling between the subducting and the overriding plates. Our results indicate that the rate of crustal shortening in the Andes has decreased with time (duing the past 26 m.y.) as a result of the thickening of the crust.

Acknowledgments. We would like to thank J. P. Vilotte, an anonymous reviewer, Bruce Buffett, Carl Gable, Winston Tao, and Joann Stock for helpful comments. We also thank Teresa Jordan and Brian Isacks for sharing with us their knowledge about the Andean tectonics. This work was supported by NASA grant NAG5-840 and NSF grant EAR-8903912.

REFERENCES

Barazangi, M., and B. L. Isacks, Spatial distribution of earthquakes and subduction of the Nazca plate beneath South America, *Geology, 4*, 686–692, 1976.

Bevis, M., Seismic slip and down-dip strain rates in Wadati-Benioff zones, *Science, 240*, 1317–1319, 1988.

Bird, P., and J. Baumgardner, Fault friction, regional stress, and crust-mantle coupling in southern California from finite element models, *J. Geophys. Res., 89*, 1932-1944, 1984.

Bird, P., and K. Piper, Plane-stress finite-element models of tectonic flow in Southern California, *Phys. Earth Planet. Inter., 21*, 158-175, 1980.

Burchfiel, B. C., and G. A. Davis, Nature and controls of Cordilleran orogenesis, western United States: extensions of an earlier synthesis, *Am. J. Sci., 275-A*, 363–394, 1975.

Cathles, L. M., The viscosity of the earth's mantle, Princeton University Press, Princeton, N. J., 1975.

Coulbourn, W. T., Tectonics of the Nazca and the continental margin of western South America, 18° to 23°, *Mem. Geol. Soc. Am., 154*, 587–618, 1981.

Dalmayrac, B., and P. Molnar, Parallel thrust and normal faulting in Peru and constraints on the state of stress, *Earth Planet. Sci. Lett., 55*, 473–481, 1981.

England, P. C., and D. P. McKenzie, A thin viscous sheet model for continental deformation, *Geophys. J. R. Astron. Soc., 70*, 295-321, 1982.

England, P. C., and D. P. McKenzie, Correction to a thin viscous sheet model for the continental deformation *Geophys. J. R. Astron. Soc., 73*, 523–532, 1983.

Froidevaux, C., and B. L. Isacks, The mechanical state of the lithosphere in the Altiplano-Pyna segment of the Andes, *Earth Planet. Sci. Lett., 71*, 305–314, 1984.

Giardini, D., and J. H. Woodhouse, Horizontal Shear flow in the mantle beneath the Tonga arc, *Nature, 319*, 551–555, 1986.

Hager, B. H., and R. J. O'Connell, Kinematic models of large scale flow in the Earth's mantle, *J. Geophys. Res., 84*, 1031–1048, 1979.

Hager, B. H., and R. J. O'Connell, A simple global model of plate motions and mantle convection, *J. Geophys. Res., 86*, 4843–4867, 1981.

Hamilton, W., Mesozoic California and underflow of Pacific mantle, *Geol. Soc. Am. Bull., 80*, 2409–2430, 1969.

Houseman, G. A., and P. C. England, Finite strain calculations of continental deformation: I. Method and general results for convergent zone, *J. Geophys. Res., 91*, 3651–3663, 1986.

Isacks, B. L., Uplift of the central Andean Plateau and bending of the Bolivian Orocline, *J. Geophys. Res., 93*, 3211–3231, 1988.

Isacks, B. L., and P. Molnar, Mantle earthquake mechanisms and the sinking of the lithosphere, *Nature, 223*, 1121–1124, 1971.

James, D. E., Andean crustal and upper mantle structure, *J. Geophys. Res., 76*, 3246–3271, 1971.

Jischke, C. J., On the Dynamics of descending lithospheric plates and slip zones, *J. Geophys. Res., 80*, 4809–4813, 1975.

Jordan, T. E., B. L. Isacks, R. W. Allmendinger, J. A. Brewer, V. A. Ramos, and C. J. Ando, Andean tectonics related to geometry of subducted Nazca plate, *Geol. Soc. Am. Bull., 94*, 341–361, 1983.

Kanamori, H., The state of stress in the earth's lithosphere, in: *Physics of the earth interior*, edited by A. M. Dziewonski and E. Boschi, North-Holland Publishing Company, Amsterdam, 531-554, 1980.

Karig, E. D., Tectonic erosion at trenches, *Earth Planet. Sci. Lett., 21*, 209–212, 1974.

Kulm, L. D., R. A. Prince, W. French, S. Johnson, and A. Masias, Crustal structure and tectonics of central Peru continental margin and trench, Nazca Plate: Crustal formation and Andean convergence, *Mem. Geol. Soc. Am., 154*, 445–468, 1981.

McKenzie, D., J. Roberts, and N. Weiss, Numerical models of convection in the earth's mantle, *Tectonophysics, 19*, 89–103, 1973.

Molnar, P., and H. Lyon-Caen, Some simple physical aspects of the support, structure, and evolution of mountain belts, *Spec. Pap. Geol. Soc. Am., 218*, 179–207, 1988.

Pardo-Casas, F., and P. Molnar, Relative motion of the Nazca (Farallon) and South America plates since Late Cretaceous time, *Tectonics, 6*, 233–248, 1987.

Peltier, W. R., and J. T. Andrews, Glacial-isostatic adjustment. I. The forward problem, *Geophys. J. R. Astron. Soc., 46*, 605–646, 1976.

Sébrier, M., J. L. Mercier, F. Mégard, G. Laubacher, and E. Carey-Gailhardis, Quaternary normal and reverse faulting and the state of stress in the central Andes of south Peru, *Tectonics, 4*, 739–780, 1985.

Sheffels, B. M., Lower bound on the amount of crustal shortening in the central Bolivian Andes, *Geol., 18*, 812–815, 1990.

Sheffels, B., B. C. Burchfiel, and P. Molnar, Deformation style and crustal shortening in the Bolivian Andes (abstract), *Eos Trans. AGU, 44*, 1241, 1986.

Stauder, W., Subduction of the Nazca Plate under Peru as evidenced by focal mechanisms and by seismicity, *J. Geophys. Res., 80*, 1053–1064, 1975.

Suárez, G., P. Molnar, and B. C. Burchfiel, Seismicity, fault plane solutions, depth of faulting, and active tectonics of the Andes of Peru, Ecuador, and southern Colombia, *J. Geophys. Res., 88*, 10,403–10,429, 1983.

Tapponier, P., and P. Molnar, Slip-line theory and large-scale continental tectonics, *Nature, 264*, 319–324, 1976.

Thorpe, R. S., P. W. Francis, and R. S. Harmon, Andean andesites and crustal growth, *Philos. Trans. R. Soc. London., Ser. A, 301*, 305–320, 1981.

Turcotte, D. L., and E. R. Oxburgh, A fluid theory for the deep structure of the dip-slip fault zone, *Phys. Earth Planet. Inter., 1*, 381–386, 1968.

Turner, J. S., Buoyancy effects in fluids, Cambridge University Press, New York, 1973.

Uyeda, S., and H. Kanamori, Back arc opening and the mode of subduction, *J. Geophys. Res., 84*, 1049–1061, 1979.

Vilotte, J. P., M. Daigniére, and R. Madariaga, Numerical modeling of intraplate deformation: Simple mechanical models of continental collision, *J. Geophys. Res., 87*, 10,709–10,728, 1982.

Vilotte, J. P., M. Daigniére, R. Madariaga, and O. Zienkiewicz, Numerical study of continental collision: Influence of buoyancy forces and an initial stiff inclusion, *Geophys. J. R. Astron. Soc., 84*, 279–310, 1986.

von Huene R., et al., Results of leg 112 drilling, Peru continental margin: part 1, Tectonic history, *Geology, 16*, 1934–939, 1988.

Walcott, R. I., Flexural rigidity, thickness, and viscosity of the lithosphere, *J. Geophys. Res., 75*, 3941–3954, 1970.

Wdowinski, S., and R. J. O'Connell, Dynamically supported trench topography, accretion, and tectonic erosion: A viscous flow model of an overriding plate sheared by a subducting slab (abstract), *Eos Trans. AGU, 71*, 1575, 1990.

Wdowinski, S., R. J. O'Connell, and P. C. England, A continuum model of continental deformation above subduction zones: Application to the Andes and the Aegean, *J. Geophys. Res., 94*, 10,331–10,346, 1989.

Zienkiewicz, O. C., The Finite Element Method, 3rd ed., McGraw-Hill, New York, 1977.

Zienkiewicz, O. C., The Finite Element Method, vol. 1, 4th ed., McGraw-Hill, New York, 1988.

R. J. O'Connell, Department of Earth and Planetary Sciences, 20 Oxford street, Cambridge MA 02138.

S. Wdowinski, Institute for Geophysics and Planetary Physics, Scripps Institution of Oceanography, University of California, San Diego, La Jolla, CA, 92093-225.

(Received June 25, 1990;
revised February 14, 1991;
accepted March 19, 1991.)